*Int. J. Electrochem. Sci.*, 13 **(2018)** 10539 – 10547, doi: 10.20964/2018.11.18

**International Journal of ELECTROCHEMICAL SCIENCE**
www.electrochemsci.org

# Facile Synthesis of $Ni_3S_2$@$MoS_2$ Nanowire Arrays Grown on Ni Foam for High Performance Supercapacitor

*Tao Han*[1,*], *Guizheng Guo*[1], *Yang Wei*[1], *Yinghe Zhang*[2], *Youyi Sun*[1]

[1] School of Materials Science and Engineering, North University of China, Taiyuan 030051,People's Republic of China
[2] Nanotechnology Department, Helmholtz Association, Hamburg 21502, Germany.
[*]E-mail: syyi2010@163.com or nucceramic@163.com

*Received:* 3 July 2018 / *Accepted:* 21 August 2018 / *Published:* 1 October 2018

Here, a novel $Ni_3S_2$@$MoS_2$ nanowire arrays grown on Ni foam was successfully synthesized by one-step hydrothermal method. At the same time, the diameter of $Ni_3S_2$@$MoS_2$ nanowire grown on Ni foam was easily controlled by the reaction times. Furthermore, the electrochemical properties of $Ni_3S_2$@$MoS_2$ nanowire arrays grown on Ni foam were analyzed and compared by the cyclic voltammetry, galvanostatic charge-discharge and electrochemical impedance spectroscopy. It was found that the capacitive properties of $Ni_3S_2$@$MoS_2$ nanowire arrays grown on Ni foam were related to the diameter of $Ni_3S_2$@$MoS_2$ nanowire. The composite foam containing $Ni_3S_2$@$MoS_2$ nanowire with diameter of ca.320.0nm showed high rate capability of 10.8 F $cm^{-2}$ at 5.0mA $cm^{-2}$ and good cycle stability with capacitance retention of 83.0% after 1000 cycles. The capability was obviously higher comparing to others $Ni_3S_2$ grown on Ni foam reported in previous works. These results implied that the design of $Ni_3S_2$@$MoS_2$ grown on Ni foam without polymer binder was an ideal candidate for supercapacitor applications.

**Keywords:** $Ni_3S_2$@$MoS_2$, Ni foam, Nanowires, hydrothermal method, Supercapacitor.

## 1. INTRODUCTION

$Ni_3S_2$ grown on Ni foam as a kind of promising electrode has attracted lots of attentions due to their good electrochemical performance for application in energy storage devices (e.g. batteries and supercapacitors) [1-2]. For example, Qi et al reported synthesis and electrochemical performance of $Ni_3S_2$ hierarchical dendrites with a three-dimensional (3D) framework, which showed high specific capacitance of 710.0F $g^{-1}$ at current density of 2.0A $g^{-1}$[1]. Kim et al reported the preparation of nest like $Ni_3S_2$ grown on Ni foam by a one-pot hydrothermal route, which showed a maximum specific capacitance of 1293.0F $g^{-1}$ at current density of 5.0mA $cm^{-2}$[2]. It was well-known that one-

dimensional (1D) nanostructure was advantageous in energy storage devices because of efficient ions and electrons transport pathways and was not easily pulverized or broken due to its facile strain relaxation, which could be effective against the volume change during electrochemical reaction[3]. Therefore, to achieve better electrochemical performance, it is highly desirable to synthesis of 1D $Ni_3S_2$ nanowire arrays grown on Ni foam. However, studies of 1D $Ni_3S_2$ nanowire arrays grown on Ni foam for application in supercapacitors have few reported. In addition to this, the electrochemical performances of $Ni_3S_2$ grown on Ni foam could be remarkably improved by combining $Ni_3S_2$ with other metal oxides $Ni(OH)_2$, $NiCo_2O_4$, $CoxS_y$, $MoS_2$ or conductive materials (rGO) to form hybrid heterostructures for application in electrodes of supercapacitor[1-2, 4-11].

Herein, $Ni_3S_2$@$MoS_2$ nanowire arrays grown on Ni foam was synthesized by a facile one-step solution method. The novel hierarchical nanostructures have the following three major merits: (1) the $Ni_3S_2$@$MoS_2$ was directly grown on Ni foam without any conductive agents and polymer binders, reducing contact resistance; (2) the porous $Ni_3S_2$@$MoS_2$ nanoarrays were directly grown on Ni foam with 3D network structure, reducing aggregation of $Ni_3S_2$@$MoS_2$ and enhancing active surface area; (3) $Ni_3S_2$@$MoS_2$ nanowire arrays were directly grown on Ni foam with 3D network, faciliting the transportation of electrolyte ions and buffering the volume change during charge/discharge process.These characters provided an excellent capacitive performance and stability over a large number of charge-discharge cycles, which was expected to apply in energy storage devices.

## 2. EXPERIMENTAL

### *2.1 Preparation of $Ni_3S_2$@$MoS_2$ nanowire arrays grown on Ni foam ($Ni_3S_2$@$MoS_2$/NF)*

The Ni foam (2.0cm×3.5cm) was dealt with 3.0M HCl solution and ultrasonically cleaned for 15.0min. After that, the Ni substrate was washed with deionized water and ethanol for several times, respectively. 0.242g sodium molybdate and 0.182g cetyl trimethyl ammonium bromide (CTAB) was dissolved in 30.0ml ethanol and water mixing solution ($CH_3CH_2OH$:$H_2O$=1:1) and then 0.153g thiourea was added into the above mixing solution. After stirring for ca. 15.0min, the above reaction solution and Ni foam was moved to a 100.0ml Teflon-lined stainless steel autoclave, which was reacted at 180.0℃ for 6.0h, 18.0h and 24.0h. After the autoclave cooled to room temperature, the samples were washed by deionized water and ethanol for several times and dried at 60.0℃ for 5.0h.

### *2.2 Characterization*

X-ray diffraction (XRD) patterns were carried out on a D/MaxRB X-ray diffractometer (Japan) using Cu-Kα radiation (λ=1.5418Å). The morphology of composite foam was taken by Scanning electron microscopy (SEM) (Su-8010, HITACHI Japan). X-ray photoelectron spectroscopy (XPS) data was done by a Thermo ESCALAB 250 system with Al-Kα source.

*2.3 Electrochemical characterization*

The electrochemical tests of supercapactior such as the cyclic voltammetry (CV), galvanostatic charge-discharge analysis (GCD) and electrochemical impedance spectroscopy (EIS) were carried out by an electrochemical workstation (CHI660C, Chenhua, Shanghai) with KOH solution (6.0M) as the electrolyte. In a three-electrode system, the $Ni_3S_2$@$MoS_2$ composite foam (1.0$cm^2$) was directly used as the working electrode, while platinum plate and Hg/HgO electrode (SCE) were served for the counter, and reference electrode. During the charge-discharge process, the specific capacitance was calculated according to the equation: $Cs$(F $cm^{-2}$) $=I\Delta t/\Delta E \times S$, where $I$ (A) is the current, $\Delta t$ (s) represents the discharge time , $\Delta E$ is the potential change (V) and $S$ ($cm^2$) is the area of active material.

## 3. RESULTS AND DISCUSSION

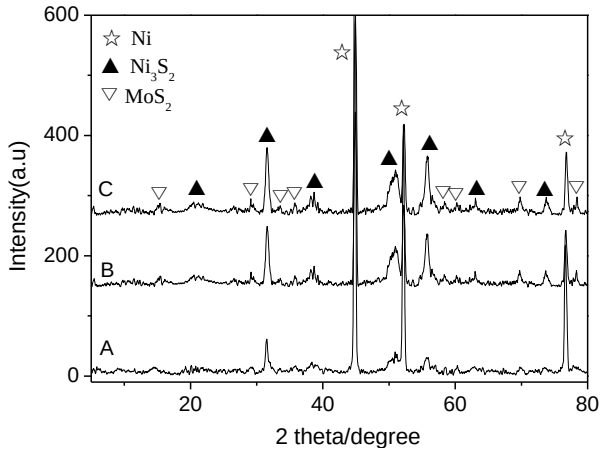


**Figure 1.** XRD of $Ni_3S_2$@$MoS_2$/NF prepared with various reaction times of (A) 6.0h, (B) 18.0h and (C) 24.0h.

The XRD patterns of $Ni_3S_2$@$MoS_2$/NF prepared with various reaction times were shown in Fig.1. It clearly showed three peaks at 44.9°, 52.1° and 76.6°, corresponding to the diffractions of (111), (200) and (220) planes of Ni, respectively (JCPDS card No. 04-0850) for all samples [12]. At the same time, excluding the diffraction peaks of Ni foam, there were others diffraction peaks located at 20°, 31.6°, 38.4°, 49.8°, 50.9°, 55.7° and 73.6° , which were indexed to the diffractions of (101), (110), (003), (113), (211), (122) and (214) planes of $Ni_3S_2$ (JCPDS no. 44-1418) [1-2]. In addition to this, the diffraction peaks at 14.2°, 29.1°, 33.5°, 35.9°, 58.4°, 60.1°, 69.7° and 78.3° were ascribed to the (002), (004), (101), (012), (110), (113), (108) and (109) planes of $MoS_2$ (JCPDS card no. 37-1492)[13]. These peaks were broad and weak, indicating that the crystallinity of the $MoS_2$ and $Ni_3S_2$ was relatively poor due to relatively low reaction temperature. These results further confirmed the formation of $Ni_3S_2$@$MoS_2$ /NF.

The XPS was further employed to identify the formation and chemical composition of $Ni_3S_2$@$MoS_2$/NF as shown in Fig.2. The pattern peaks of Ni, Mo, S, C and O elements were clearly observed, revealing the existence of these elements. In Fig.2B, the Ni2p spectrum of the $Ni_3S_2$@$MoS_2$/NF displayed two peaks at 855.7eV and 873.4eV, which was belonged to $Ni2p_{3/2}$ and Ni

$2p_{1/2}$ [5], respectively. As seen in Fig.2C, the two peaks at 229.4eV and 232.5eV corresponded to Mo $3d_{5/2}$ and $Mo3d_{3/2}$, which were attributed to $Mo^{4+}$ in $MoS_2$[14]. Fig.2D showed the S2p spectrum, in which the binding energy at 168.4eV could be fitted by one main peak and one shakeup satellite peak[15]. The strong peaks at around 162.4eV and 161.6eV corresponded to $S2p_{1/2}$ and $S2p_{3/2}$, respectively [5]. In Fig.2A, the peak at 284.7eV was assinged to the binding energy of C1s. What's more, the peak at 530.5eV was assigned to O1s because the oxygen would adsorb on the surfaces of the products [16].

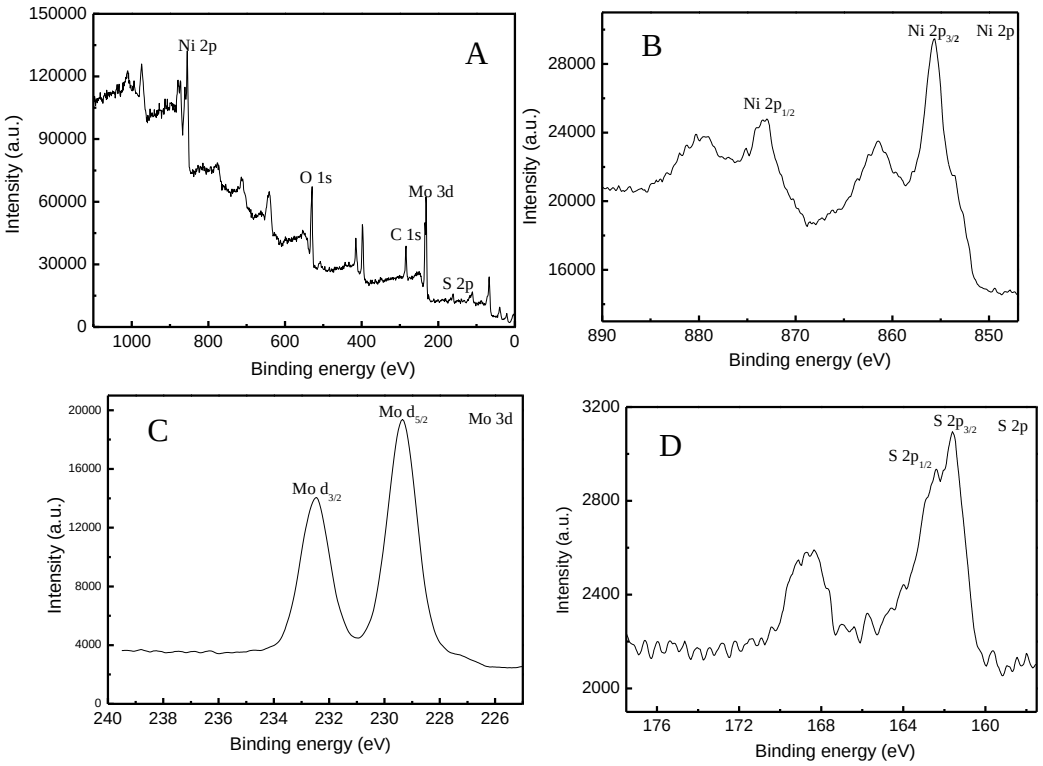


**Figure 2.** XPS spectra of $Ni_3S_2$@$MoS_2$/NF prepared with reaction time of 18.0h. (A) Survey spectrum of composite foam, (B) Ni2p spectrum, (C) Mo3d spectrum and (D) S2p spectrum.

The morphology of $Ni_3S_2$@$MoS_2$/NF prepared with various reaction times was investigated by the SEMs as shown in Fig.3. The inset in Fig.3A displayed the optical images of the neat Ni foam and $Ni_3S_2$@$MoS_2$/NF. The surface color of the Ni foam changed from silver white to black demonstrated the deposition of $Ni_3S_2$@$MoS_2$ on Ni foam. As shown in Fig.3A-C, the thin and dense $Ni_3S_2$@$MoS_2$ layer was uniformly coated on the skeleton of Ni foam with highly open porous 3D network structure for all samples. At higher magnification (in Fig.3D-F), it clearly showed that the $Ni_3S_2$@$MoS_2$ layer grown on Ni foam were composed of nanowire arrays. At the same time, it showed that the diameter of $Ni_3S_2$@$MoS_2$ nanowire grown on Ni foam increased with increasing reaction time. At the reaction time of 6.0h, the diameter of nanowire was about 74.0nm, and when the reaction time was increased to 24.0h, the diameter of nanowire was about 360.0nm. These results indicated that the porous $Ni_3S_2$@$MoS_2$/NF could be prepared by the simple method, which was suited to application in energy storage.

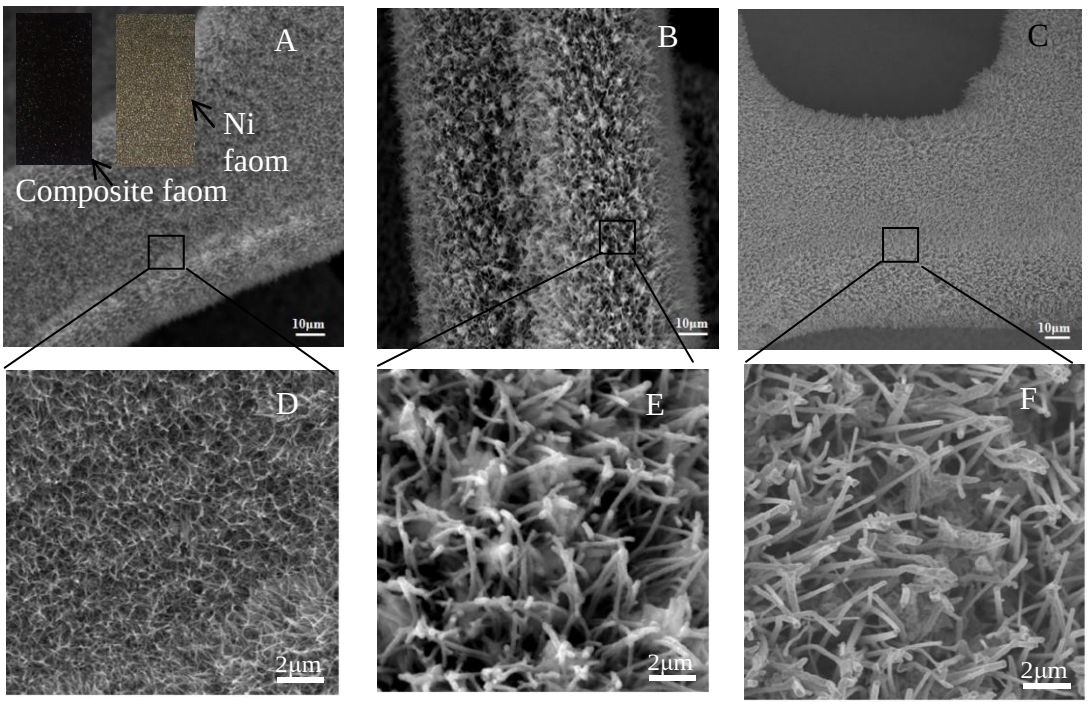


**Figure 3.** SEM images of the $Ni_3S_2$@$MoS_2$/NF prepared with various reaction times of (A) 6.0h, (B) 18.0h and (C)24.0h. The inset of (A) is the optical photograph of neat Ni foam and $Ni_3S_2$@$MoS_2$/NF. (D), (E) and (F) are the enlarged view of the black square dashed box marked in (A), (B) and (C), respectively.

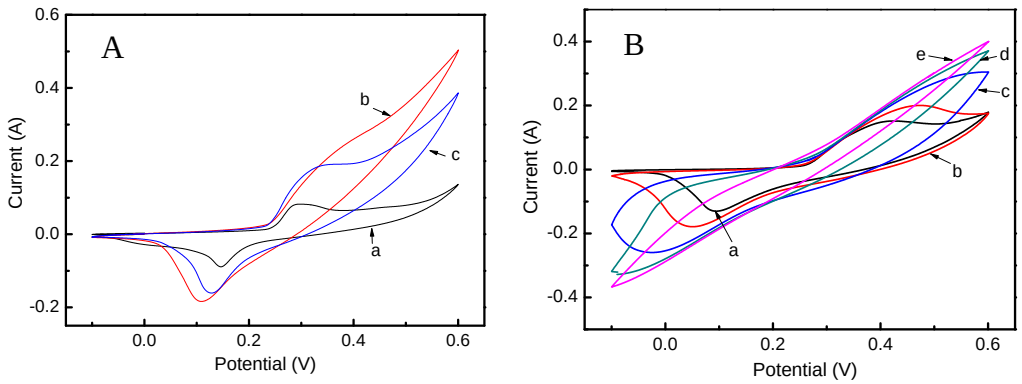


**Figure 4.** (A) The CV curves of the $Ni_3S_2$@$MoS_2$/NF prepared with various reaction times of (a) 6.0h, (b)18.0h and (c) 24.0h at 5.0mV $s^{-1}$, (B) the $Ni_3S_2$@$MoS_2$ nanowire array grown on Ni foam at different scan rates of (a) 5.0mV $s^{-1}$, (b) 10.0mV $s^{-1}$, (c) 25.0mV $s^{-1}$, (d) 50.0mV $s^{-1}$ and (e) 100.0 mV $s^{-1}$.

Fig.4A shows the CV curves of $Ni_3S_2$@$MoS_2$/NF in the potential window of -0.1V~0.6V at the scanning rate of 5.0mV $s^{-1}$. The CV curves of all composite foams exhibited nearly a couple of redox peaks, indicating the Faradaic capacitive behavior [17]. More importantly, the CV area of the $Ni_3S_2$@$MoS_2$/NF prepared with reaction time of 18.0h was larger than that of other $Ni_3S_2$@$MoS_2$/NF prepared with reaction time of 6.0h and 24.0h. The results suggested that the $Ni_3S_2$@$MoS_2$/NF prepared with reaction time of 18h showed a larger specific capacitance comparing to the other

$Ni_3S_2$@$MoS_2$/NFs[18]. Fig. 4B shows the CV curves of the $Ni_3S_2$@$MoS_2$/NF prepared with reaction time of 18.0h at various scan rates. It could be seen that $Ni_3S_2$@$MoS_2$/NF displayed relatively rectangular CV curves at relatively low scan rate (5.0mV $s^{-1}$), indicating a nearly ideal supercapacitor behavior. Even at high scan rate of 50.0mV $s^{-1}$, the CV curve still clearly showed a pair of redox peaks. These results further indicated that the hierarchical nanowire array composed of porous nanowires was beneficial to fast charge-discharge due to the high interface area, easy ion diffusion, low resistance and super-fast electronic transport rate between the nanowire and Ni current collector.

The GCD profiles of the $Ni_3S_2$@$MoS_2$/NFs were also characterized at a scan rate of 5.0mA $cm^{-2}$ as shown in Fig. 5A. All composite foams exhibited a symmetrical and closely no-linear slope during charging and discharging processes, suggesting a good supercapacitor behavior [7]. As seen, the specific capacitance of the $Ni_3S_2$@$MoS_2$/NF prepared with reaction time of 18.0h was about 10.8F $cm^{-2}$ at a scan rate of 5.0mA $cm^{-2}$, and was higher than that (5.1F $cm^{-2}$) and (9.4F $cm^{-2}$) of $Ni_3S_2$@$MoS_2$/NF with reaction time of 6.0h and 24.0h, respectively. Moreover, these were much higher than the specific capacitance of other electrodes based on $Ni_3S_2$/NF as shown in Table 1[2, 4-7].

**Table 1.** The comparison in capacitve properties of electrodes based on $Ni_3S_2$/NF

| Sample | Capacitance/F $cm^{-1}$ (current density) | high-rate retention/% (increasing times ) | Cycle retention/% (cycle times) | Re. |
|---|---|---|---|---|
| $Ni_3S_2$@$MoS_2$/NF | 10.8 (5.0mA $cm^{-1}$) | 75.0 (4.0 times) | 83.0 (1000.0 times) | present |
| $Ni_3S_2$/NF | 7.8(5.0mA $cm^{-1}$) | 58.5 (4.0 times) | 69.0 (1000.0 times) | [2[ |
| $Ni_3S_2$@rGO/NF | 7.4(10.0mA $cm^{-1}$) | 46.0 (10.0 times) | 90.1 (1000.0 times) | [5] |
| $Ni_3S_2$@$Ni(OH)_2$/NF | 3.7(19.8mA $cm^{-1}$) | 38.3 (4.0 times) | 99.1 (2000.0 times) | [6] |
| $Ni_3S_2$@$NiCo_2O_4$/NF | 3.6(2.1mA $cm^{-1}$) | 64.0 (10.0 times) | 83.7 (2000.0 times) | [7] |
| $Ni_3S_2$@CoS/NF | 4.9(4.0mA $cm^{-1}$) | 72.8(4.0 times) | 98.8 (1000.0 times) | [8] |

Fig.5B shows the charge-discharge properties of the $Ni_3S_2$@$MoS_2$/NF prepared with reaction time of 18.0h at different current densities. The specific capacitance could reach as high as 10.8F $cm^{-1}$, 12.6F $cm^{-1}$, 8.1F $cm^{-1}$, 6.4F $cm^{-1}$ and 5.2F $cm^{-1}$ at 5.0mA $cm^{-2}$, 10.0mA $cm^{-2}$, 20.0mA $cm^{-2}$, 30.0mA $cm^{-2}$ and 40.0mA $cm^{-2}$, respectively. When the current density was increased to 40.0mA $cm^{-2}$, the specific capacitance of the $Ni_3S_2$@$MoS_2$/NF decreased to 5.2F $cm^{-1}$ which was about 48.1% of that measured at 5.0mA $cm^{-1}$, indicating that this material had a relatively good rate capability. Fig.5C shows the cycling performance of the $Ni_3S_2$@$MoS_2$/NF at 5.0mA $cm^{-2}$. The specific capacitance slightly decreased with the cycling number and 83.0% of initial capacitance could be remained after 1000.0 cycles. These results indicated that the porous $Ni_3S_2$@$MoS_2$/NF exhibited also a good cycling stability. These results were mainly attributed to the synergetic effect between $Ni_3S_2$ and $MoS_2$. In addition to this, the $Ni_3S_2$@$MoS_2$ nanowire array also played important role. It was conducive to the electrolyte infiltrating into electrode and leading to a high availability of active materials.

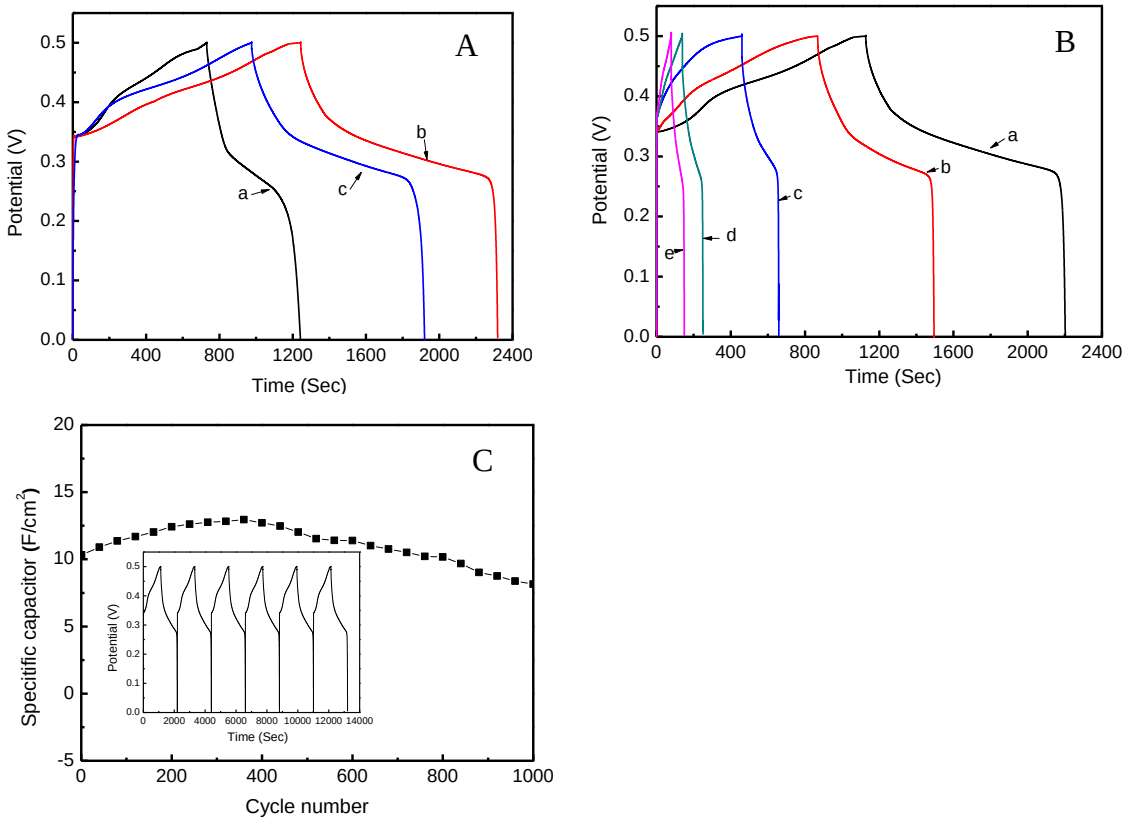


**Figure 5.** (A) The GCD curves of the $Ni_3S_2$@$MoS_2$/NF prepared with various reaction times of (a) 6.0h, (b)18.0h and (c) 24.0h at current density of 5.0mA $cm^{-2}$, (B) The GCD curves of the $Ni_3S_2$@$MoS_2$/NF prepared with reaction time of 18.0h at various current densities of 5.0mA $cm^{-2}$, 10.0mA $cm^{-2}$, 20.0mA $cm^{-2}$, 30.0mA $cm^{-2}$ and 40.0mA $cm^{-2}$, (C) is cycling performance of $Ni_3S_2$@$MoS_2$/NF prepared at 18.0h measured at a current density of 5.0mA $cm^{-2}$.

In order to study the mechanism of $Ni_3S_2$@$MoS_2$/NF with good capacitive performance, the EIS of all composite foams were also characterized as shown in Fig.6., The impedance plot at the low-frequency region was vertical lines, indicating the pure capacitive behavior [17]. At the high frequency, the intercept at real axis (*Z'*) represented the equivalent series resistance (ESR), resulting from ionic resistance of electrolyte, intrinsic resistance of substrate and contact resistance at the interface of active material/current collector [19]. The semicircle represented the charge transfer resistance (Rct), resulting from the contact resistance at the electrode/electrolyte interface. The ESR of $Ni_3S_2$@$MoS_2$/NF prepared with various reaction times of 6.0h, 18.0h and 24.0h were about 0.79Ω, 0.78Ω and 0.77Ω, implying that the effect of reaction time on intrinsic resistance and contact resistance of $Ni_3S_2$@$MoS_2$/NF was slight. Furthermore, a semicircle was almost not observation, indicating the low Rct and a short path of the ion diffusion for all samples[20-21]. Here, the low ESR and Rct value of $Ni_3S_2$@$MoS_2$/NF was attributed to intrinsic characteristics of $Ni_3S_2$@$MoS_2$ nanowire array, which was beneficial to create a pathway for charge storage and electrolyte diffusion. The $Ni_3S_2$@$MoS_2$ nanowire array was directly used as work electrode of supercapacitor, which effectively provided a highway for electron transportation.

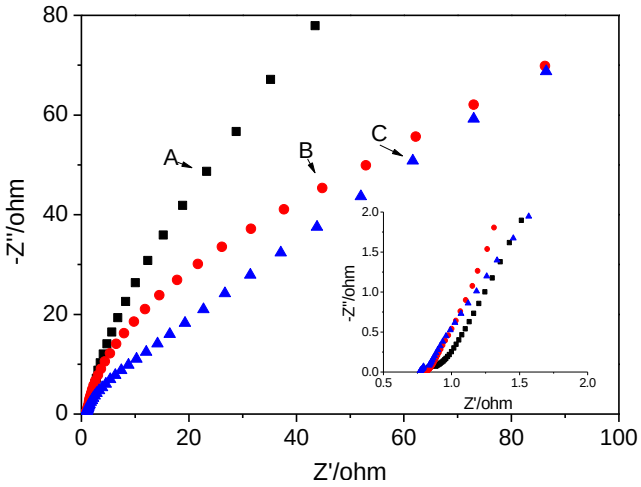


**Figure 6.** Nyquist plots of the $Ni_3S_2$@$MoS_2$/NF prepared with various reaction times of (A) 6.0h, (B) 18.0h and (C) 24.0h . The inset is an enlarged curve of the high frequency region.

## 4. CONCLUSIONS

In summary, a simple hydrothermal method was used to prepare $Ni_3S_2$@$MoS_2$ nanowire arrays grown on Ni foam, in which size of $Ni_3S_2$@$MoS_2$ nanowire could be easily controlled by adjusting the reaction times. Moreover, the $Ni_3S_2$@$MoS_2$ nanowire grown on Ni foam showed excellent capacitive performance of 12.6F $cm^{-2}$ at a current density of 10.0mA $cm^{-2}$. The composite foam owed to homogenous coverage of $Ni_3S_2$@$MoS_2$ nanowire array on Ni foam, facilitating the faster ions transport and the electrochemical utilization of $Ni_3S_2$-$MoS_2$ nanowires. Besides, it was related to the intrinsic nature of the low Rct and ESR, and a short path of the ion diffusion. The enhanced electrochemical behaviors of the $Ni_3S_2$@$MoS_2$ hybrids might bring about promising for high-performance supercapacitors.

ACKNOWLEDGEMENTS
The authors thank the ShanXi Provincial Natural Science Foundation of China (No: 2015011016), Shanxi Province Key Laboratory of Higee-Oriented Chemical Engineering (No: CZL201505)for the financial support.

## References

1. Z. Zhang, Z.Y Huang, L. Ren, Y.Z. Shen, X. Qi and J.X. Zhong, *Electrochim.Acta.*, 149 (2014) 316.
2. K.Krishnamoorthy, G.K. Veerasubramani, S. Radhakrishnan and S.J. Kim, *Chem.Eng. J.*, 251 (2014) 116.
3. S.Y.Jeong, S.K.Park, Y.C.Kang and J.S.Cho. *Chem. Eng. J.* 351 (2018) 559.
4. J.Wang, D.L. Chao, J.L.Liu, L.L. Li, L.F. Lai, J.Y. Lin and Z.X. Shen, *Nano Energy*.,7(2014) 151.
5. Z.M.Zhang, C.J. Zhao, S.D.Min and X.Z. Qian, *Electrochim.Acta.*, 144 (2014) 100.
6. W.J. Zhou, X.H. Cao, Z.Y. Zeng, W.H. Shi, Y.Y. Zhu, Q.Y. Yan, H. Liu, J.Y. Wang and H. Zhang, *Energy Environ. Sci.*, 6(2013)2216.
7. J.P.Wang, S.L. Wang, Z.C. Huang and Y.M.Yu, *J. Mater. Chem. A.*, 2(2014)17595.
8. R. Li, S.L. Wang, J.P. Wang and Z.C. Huang, *Phys. Chem. Chem. Phys.*,17*(* 2015)16434.
9. D.Ghosh and C.K.Das, *ACS Appl. Mater. Interfaces.*, 7(2015)1122.

10. Z.M. Zhang, Q. Wang and C.J. Zhao, *ACS Appl. Mater. Interfaces*., 7(2015)4861.
11. C.J. Zhao, Z.M. Zhang, Q. Wang, S.D. Min and X.Z. Qian, *RSC Adv.*, 5(2015)63528.
12. Y.Y.Sun,W.H. Zhang, Di.S.Li, L. Gao, C.L. Hou,Y.H. Zhang and Y.Q.Liu, *Electrochim.Acta.*, 178(2015)823.
13. K.Fan, Z.L.Jin, G.R.Wang, H.Yang, D.D.Liu, H.Y. Hu, G.X. Lu and Y.P. Bi, *Catal. Sci. Technol.*, 8(2018)2352.
14. M.C. He, F.P. Kong, G.P. Yin, Z. Lv, X.D.Sun, H.Y. Shi and B. Gao, *RSC Adv.*, 8(2018)14369.
15. C.X.Wang, J.L. Jin, Y.Y. Sun, J.R.Yao, G.Z.Zhao and Y.Q. Liu, *Chem. Eng. J.*, 327(2017)774.
16. S.Yang, M.X.Hua, L. Shen, X.L. Han, M.Y. Xu, L.J.Kuang and D.B. Hua, *J. Hazard.Mater.*, 354 (2018) 191.
17. W.H. Zhang, Y.Y. Sun, T.T. Liu, D.S. Li, C.L. Hou, L. Gao and Y.Q. Liu, *Applied Physics A.*, 122(2016)259.
18. Y.Y.Sun, W.H. Zhang, D.S. Li, L. Gao, C.L. Hou, Y.H.Zhang and Y.Q. Liu, *J.Alloy.Compd.*, 649(2015)579.
19. H.Zhang, Y.Y.Zhou, Y.B.Ma, J.R.Yao, X. Li, Y.Y. Sun, Z.Y. Xiong and D.Li, *J.Alloy. Compd.*,740 (2018) 174.
20. A.A.Memon, S.A. Patil, K.C. Sun, N. Mengal, A. A.Arbab, I.A.Sahito, S. H. Jeong and H. S. kim, *Electrochim.Acta.*, 283 (2018) 997.
21. L.S.Yang, Y. Liu, J.B. Li and G.P. Du, *J. Alloy. Compd.*, 763(2018)134.